Wake meandering under non-neutral atmospheric stability conditions – theory and facts

Larsen, Gunner Chr.; Machefaux, Ewan; Chougule, Abhijit S.

Published in:
Journal of Physics: Conference Series (Online)

Link to article, DOI:
10.1088/1742-6596/625/1/012036

Publication date:
2015

Document Version
Publisher's PDF, also known as Version of record

Wake meandering under non-neutral atmospheric stability conditions - theory and facts

2015 J. Phys.: Conf. Ser. 625 012036

(http://iopscience.iop.org/1742-6596/625/1/012036)

Wake meandering under non-neutral atmospheric stability conditions – theory and facts

G C Larsen[1], **E Machefaux and A Chougule**
Department of Wind Energy, Technical University of Denmark
P.O. Box 49, 4999 Roskilde, Denmark

E-mail: gula@dtu.dk

Abstract. This paper deals with modelling of wake dynamics under influence of atmospheric stability conditions different from neutral. In particular, it is investigated how the basic split in turbulent scales, on which the Dynamic Wake Meandering model is based, can be utilized to include atmospheric stability effects in this model. This is done partly by analyzing a large number of turbulence spectra obtained from sonic measurements, partly by analyzing dedicated full-scale LiDAR measurements from which wake dynamics can be directly resolved. The theory behind generalizing the Dynamic Wake Meandering model to non-neutral conditions are summarized and linked to the results of the full-scale experimental results. It is concluded that there is a qualitative match between the conjecture behind the Dynamic Wake Meandering model and the dependence of turbulence structure on atmospheric stability conditions, and consequently that there is a potential for generalizing the Dynamic Wake Meandering model to include effects of atmospheric stability.

1. Introduction

Wakes cause significant power losses in wind farms. On average these losses amount to 10 - 20% of the wind farm power output. In addition to the power losses comes the increased (fatigue) loading of turbines operated under wake conditions, and wakes are therefore a major factor in wind farm economics. Wake effects relate to a multitude of aspects related to the interplay between wind farm topology and site wind field characteristics such as mean wind speed distribution, wind direction distribution, atmospheric turbulence and atmospheric stability [1], [2].

This paper deals with modelling of wake dynamics under influence of atmospheric stability conditions different from neutral and addresses thereby both power and load predictions of turbines located in wind farms under such conditions. Whereas friction is dictating the structure of turbulence in the atmospheric boundary layer (ABL) under neutral conditions, buoyancy effects adds to friction when it comes to the turbulence structure under ABL stability conditions different from neutral.

The major impact from buoyancy on the ABL turbulence structure is on the large turbulent scales, and being largely based on a convenient split in turbulence scales it may be straight forward to include atmospheric stability aspects into the framework of the Dynamic Wake Meandering (DWM) model [3], [4]. Crucial in this regard is if the specific scale split applied in the DWM model is such, that ABL stability affects primary the (lateral and vertical) turbulent scales, which drives the wake meandering. This is the basic conjecture on which the work in [3] and [4] is based.

[1] To whom any correspondence should be addressed.

For a variety of stability conditions, we will explore this conjecture partly by analyzing full-scale velocity measurements and partly by analyzing organized wake deficit flow structures as well as wake dynamics as based on full-scale LiDAR measurements. Finally, the performance of a newly developed spectral tensor, consistently including buoyancy effects in the ABL turbulence description [5], will be investigated.

2. Simulation of wake affected flow fields under non-neutral conditions

Buoyancy and wake affected flow fields can be modelled using advanced CFD models – e.g. CDF LES combined with actuator disc or actuator line representation of wind turbine rotors [6]. However, such simulations are computationally very demanding and consequently not yet suited for neither wind turbine design simulations nor for wind farm layout optimization. Both these disciplines call for simplified models describing the essential physics of the problem(s). One possible candidate is the DWM model ([7], [8]), which has recently been included in the IEC standard as a recommended practice, and which offers simulation of in-stationary wind farm flow fields with an acceptable computational effort.

2.1. The DWM conjecture and atmospheric stability implications

Based on a priori knowledge of the undisturbed ambient wind climate on a wind farm site, the DWM model provides detailed information of the inflow wind field to each individual wind turbine inside the wind farm. The DWM model describes the essential physics of the problem, and accounts both for the observed increased *turbulence level* of wake flow fields and for the modified *turbulence structure*. The model has successfully been verified against both full-scale measurements [9], [10] and against detailed CFD LES actuator line (ACL) computations [8].

The core of the model is a *split of scales* in the wake flow field, with large scales being responsible for stochastic *wake meandering*, and small scales being responsible for wake *attenuation* and *expansion* in the meandering frame of reference as caused by turbulent mixing. Thus, essentially the DWM model assumes that the transport of wakes in the atmospheric boundary layer (ABL) can be modeled by considering the wakes to act as passive tracers driven by a combination of large-scale turbulence structures and a mean downstream advection velocity, adopting the Taylor hypotheses. With the large turbulent structures being modeled using the Navier-Stokes (N-S) consistent Mann spectral tensor [12], and modeling of the organized wake deficits flow structures being based on the thin layer approximation of N-S in their rotationally symmetric form combined with an dedicated eddy viscosity turbulence closure, the DWM approach resembles the characteristics of a CFD Large Eddy Simulation (LES) approach and may thus be considered as the “poor man’s LES”.

While the original version of the DWM model was intended for simulation of neutrally stratified atmospheric boundary layers (ABL), the generalization to ABL stability conditions different from neutral is straight forward. This is because of the DWM spilt of scales matches nicely with the fact that the various ABL stability characteristics primarily affect the low frequency part of the turbulence spectra, and thus primarily the large-scale turbulent structures. Therefore a particular stability classification has a direct impact on the wake meandering part of the DWM formulation, whereas the small scale turbulence regime of DWM is less affected.

Within the DWM framework we consequently assume ABL stability *only* to impact the turbulent scales within the meandering regime. This was first conjectured in [11] and later further elaborated on in [4]. However, in these initial studies the approach was limited by the lack of a consistent kinematic model for turbulence modelling under non-neutral ABL stability conditions, and the Mann spectral tensor, although developed for neutral conditions, was used in approximate manner to cover also non-neutral conditions. This shortcoming has recently been overcome by the development of buoyancy dependent spectral tensor [5], whereby ABL stability effects can consistently be accounted by within the framework of the DWM model.

2.2. Buoyancy dependent spectral tensor

The generalized spectral tensor, $\Phi_{ij}(\boldsymbol{k})$, resulting from the governing Rapid Distortion Theory (RDT) equations including buoyancy effects [5], contains two extra parameters, in addition to those of the "classic" Mann spectral tensor model, where $\boldsymbol{k}(t) = (k_1, k_2, k_{30}\text{-}k_1(\mathrm{d}U/\mathrm{d}z)t)$ is a three dimensional wave vector, and t is time. These parameters are: 1) a stability parameter (the Richardson number); and 2) the rate of destruction of temperature variance.

The RDT equations, which include the linearized momentum and the temperature equation in Fourier space, evaluates in time under the influence of a constant wind shear ($\mathrm{d}U/\mathrm{d}z$) and a constant gradient of potential temperature ($\mathrm{d}\theta/\mathrm{d}z$) from an initial isotropic state of turbulence. In isotropic turbulence, the velocity-spectrum tensor is

$$\Phi_{ij}(\boldsymbol{k}_0) = \frac{E(k)}{4\pi k^2}\left(\delta_{ij} - \frac{k_i k_j}{k^2}\right),$$

where $\boldsymbol{k}_0 = \boldsymbol{k}(0)$ and k is the length of the vector $\boldsymbol{k}$. The energy spectrum, $E(k)$, is given by [13] as

$$E(k) = \alpha\varepsilon^{2/3}L^{5/3}\frac{(kL)^4}{(1+(kL)^2)^{17/6}},$$

where $\alpha \approx 1.7$ is the Kolmogorov constant, ε is the rate of viscous dissipation of specific turbulent kinetic energy (TKE), and L is a turbulence length scale.

In order to make the model stationary, the time dependency in the model is removed by incorporating the general concept of an eddy life time, $\tau(k)$. The parameterization of $\tau(k)$ is adapted from the "classic" Mann spectral tensor model [12]. In the inertial sub-range, the life time of eddies are proportional to $k^{-2/3}$, and the assumption in the Mann model, for scales larger than the inertial sub-range, is that the eddy life time is proportional to k^{-1} divided by their characteristic velocity given by

$$\left(\int_k^\infty E(p)dp\right)^{1/2},$$

thus resulting in eddy life times proportional to $k^{-2/3}$ for $k \to \infty$ and to k^{-1} for $k \to 0$.

For the temperature variable, the isotropic three-dimensional spectrum is given as

$$\Phi_{\theta\theta}(\boldsymbol{k}_0) = \frac{S(k)}{4\pi k^2},$$

where $S(k)$ is the potential temperature energy spectrum containing the form of the inertial sub-range [14] as

$$S(k) = \beta\varepsilon^{-1/3}\varepsilon_\theta L^{5/3}\frac{(kL)^2}{(1+(kL)^2)^{11/6}},$$

Here ε_θ is the dissipation rate for half the temperature variance, and $\beta = 0.8$ is a universal constant [15]. Based on the above formulations of isotropic velocity and temperature spectra combined with the Mann eddy life time formulation, RTD results in an anisotropic spectral tensor including buoyancy of the form $\Phi_{ij}(\boldsymbol{k}) = \Phi_{ij}(\boldsymbol{k}; \alpha\varepsilon^{2/3}, L, \Gamma, Ri, \eta_\theta)$, where Ri denotes the Richardson number [14] resulting from the temperature equation, and

$$\eta_\theta \equiv \frac{\varepsilon_\theta}{\varepsilon}\left[\frac{g}{\theta}\left(\frac{dU}{dz}\right)^{-1}\right]^2,$$

where the potential temperature, θ, as well as $\mathrm{d}U/\mathrm{d}z$ and $\mathrm{d}\theta/\mathrm{d}z$ are representative of the height of interest.

To summarize, the five adjustable model parameters, which are attainable from single-point measurements are: 1) $\varepsilon^{2/3}$; 2) L, which represents a representative size of the energy containing eddies; 3) Γ, which is a measure of the degree of turbulence isotropy; the Richardson number Ri [14]; and 5) η_θ as defined above. Note, that for $Ri = 0$ and $\eta_\theta = 0$, the generalized spectral tensor degenerates to the "classic" Mann spectral tensor.

Simulation of consistent 3D synthetic turbulence fields requires knowledge of cross-spectra between turbulence components. The spectral tensor model provides the cross-spectrum, χ_{ij}, between any two velocity components, or between any velocity component and temperature, as

$$\chi_{ij}\left(k_1, \Delta y, \Delta y; \alpha\varepsilon^{2/3}, L, \Gamma, Ri, \eta_\theta\right) \equiv \alpha\varepsilon^{2/3} L^{5/3} \int \Phi_{ij}\left(\boldsymbol{k}; \alpha\varepsilon^{2/3}, L, \Gamma, Ri, \eta_\theta\right) e^{\mathrm{i}(k_2\Delta y + k_3 \Delta z)} dk_2 dk_3 \,,$$

where Δy and Δz are transverse and vertical separations, respectively. Thus, based on such cross-spectra, the requested turbulence field is simulated using the approach described in [16], however, presently only implemented for the velocity components.

3. Examination and validation of basic DWM conjecture

As mentioned, the basic conjecture behind the DWM modelling of non-neutral wake affected flows is that ABL stability predominantly impacts only the turbulent scales within the meandering regime. In this section we will examine this conjecture using a 500kW example turbine. The analysis will focus on lateral turbulence characteristics, since this turbulence component is the most important regarding wake meandering. First a large number of full-scale sonic measurements are analyzed with the available data material binned with respect to both mean wind speed (1m/s bins) and ABS stability (7 stability classes). Subsequently dedicated full-scale LiDAR measurements are used to resolve and compare wake characteristics for three different stability conditions with mutually comparable inflow mean wind speeds.

3.1. Classification of ABL stability

Classification of atmospheric stability conditions is in this context based on the Monin-Obukhov length, which can be derived directly from sonic measurements. The Monin-Obukhov length, L, is defined as [14]

$$L = -\frac{u_*^{\,3}}{\kappa\left(g/T\right)\left\langle w'\Theta_v'\right\rangle} \,,$$

where g and T are respectively acceleration of gravity and absolute temperature, u_* is the friction velocity, and $\left\langle w'\Theta_v'\right\rangle$ denotes the mean kinematic virtual heat flux with w and Θ_v being the vertical components of the velocity and the virtual potential temperature, respectively. A prime denotes fluctuations, and κ is the von Kármán constant (≈ 0.4).

The Monin-Obukhov length expresses the height where production of mechanical and convective turbulence is equal, and thus offers a natural way to quantify the degree of dominance of buoyancy over mechanical and shearing effects. Adopting the classification scheme proposed in [17], the following 7 stability classes are defined:

- Very stable: $10 \leq L < 50$
- Stable: $50 \leq L < 200$
- Near neutral-stable: $200 \leq L < 500$
- Neutral: $|L| \geq 500$
- Near neutral-unstable: $-500 < L \leq -200$
- Unstable: $-200 < L \leq -100$
- Very unstable: $-100 < L \leq -50$

3.2. Full-scale sonic measurements

The measurement campaign was conducted from June 2011 to early January 2012 at the DTU Risø Campus, and sonic data recorded 16.5m a.g.l. are used for this analysis. To ensure "homogeneous" inflow conditions, only data from the (prevailing) wind direction sector (120° - 150°) is used, resulting in 1122 available 10-minute time series covering the mean wind speed regime ranging from 4-10m/s.

These data are binned with respect to mean wind speed and ALB stability. The resulting bin matrix is shown in Table 1, where the numbers reflect the number of available 10-minute time series available within each particular bin.

Table 1. Bin matrix specifying number of available 10-minute time series.

Wind speed interval [m/s]	Very unstable	Unstable	Near neutral-unstable	Neutral	Near neutral-stable	Stable	Very stable
4-5	6	2	2	12	12	68	108
5-6	40	20	12	28	28	84	90
6-7	36	12	18	58	16	26	6
7-8	38	56	44	66	12	4	0
8-9	8	12	56	60	6	0	0
9-10	0	2	4	18	0	0	0

For each bin, the power spectrum of the *lateral* turbulence component is evaluated as based on the available 10-minute time series. Prior to the spectral analysis all data have normalized with their respective mean wind speeds and de-trended assuming a linear trend. This is done to assure un-weighted averaging (assuming constant turbulence intensity within stability-wind-speed bins) in the subsequent averaging of spectra belonging to the same bin, which is performed to improve statistical significance of the spectral estimates. Aiming at investigating the spectral characteristics wind speed bin-wise, the described bin-wise normalization of spectra does not provide any restriction for the present data analysis.

Examples of bin-normalized spectra, associated with mean wind speeds in the interval [6; 7]m/s, are shown in Figure 1.

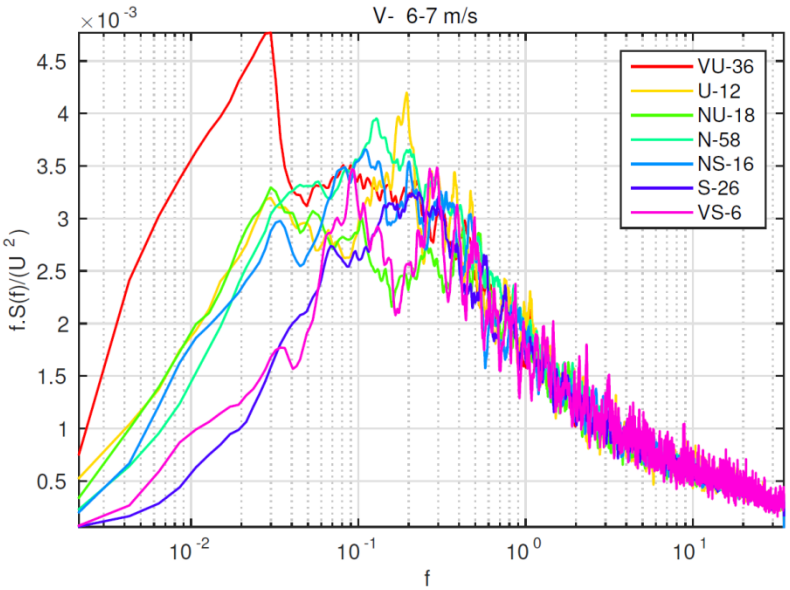

Figure 1. Normalized spectra for various stability conditions and associated with mean wind speeds in the interval [6; 7]m/s.

In neutral conditions the turbulence generation is dictated by mechanical friction. For non-neutral ABL conditions buoyancy inters the scene as an additional turbulence source term. The consequence is that *turbulence intensity* as well as *turbulence structure* varies with stability condition. As seen from Figure 1, ABL stability conditions hardly affect the spectral inertial subrange regime, but significantly alter the large scale energy-containing spectral regime [14], where the turbulent energy is produced. In the present analysis we will, as already indicated, explore non-neutral stability conditions mean wind speed bin-wise with focus on derived effects on wake meandering dynamics.

For this purpose, we will now focus on the energy balance, quantified in normalized numbers, between "large" and "small" scale turbulence as function of ABL stability condition. Analogues, we will investigate the dependence of the total spectral energy on stability conditions. To relate to the DWM split in scales [7], "large" scale turbulence is in this context defined as turbulence associated with frequencies below a frequency split given by $f_s = U/(2D)$, where U denotes the mean wind speed and D is the diameter of the rotor in question, and "small" scale turbulence in analogy defined as turbulence associated with frequencies above f_s. In the present analysis, U will refer to the *average* of 10-minute mean wind speeds belonging to a particular mean wind speed bin, and D is defined by the previously mentioned Nordtank 500kW example turbine with a rotor diameter of 41m. This turbine was selected as example turbine, because it is the turbine on which the subsequent LiDAR measurement analysis is based.

Table 2 shows the dependence of turbulence variance on ABL stability conditions for the analyzed mean wind speed bins, whereas Table 3 and Table 4 show the ABL stability dependence of "large" scale turbulence variance and of "small" scale turbulence variance, respectively.

Table 2. Bin specific variance normalized with respect to variance associated with neutral conditions.

Wind speed interval [m/s]	Very unstable	Unstable	Near neutral-unstable	Neutral	Near neutral-stable	Stable	Very stable
4-5	1,00	0,83	1,20	1,00	1,12	0,77	0,50
5-6	1,51	2,06	1,07	1,00	0,94	0,77	0,54
6-7	1,23	1,00	0,93	1,00	0,95	0,75	0,77
7-8	1,22	1,19	1,04	1,00	0,97	1,28	-
8-9	0,96	0,80	0,88	1,00	0,77	-	-
9-10	-	0,86	0,83	1,00	-	-	-

For all mean wind speed regimes Table 2 reflects, as expected, a clear trend with the turbulent energy increasing relatively for unstable ABL conditions and decreasing relatively for stable ABL conditions. As seen, this difference in energy level is up to a factor between 2 and 3 for low mean wind speeds which, however, is expected to be reduced for higher mean wind speeds, where the mechanically generated turbulence gradually increases relative to the buoyancy generated part. A few "outliers" are observed which is attributed to the limited number of statistical degrees of freedom available for spectral averaging in certain bins (cf. Table 1).

Table 3. Bin specific "large" scale variance normalized with respect to "large" scale variance associated with neutral conditions.

Wind speed interval [m/s]	Very unstable	Unstable	Near neutral-unstable	Neutral	Near neutral-stable	Stable	Very stable
4-5	1,78	1,37	2,93	1,00	0,89	0,76	0,52
5-6	2,23	3,63	1,47	1,00	0,90	0,63	0,37
6-7	1,71	1,07	1,09	1,00	0,96	0,50	0,65
7-8	1,51	1,41	1,16	1,00	0,95	1,33	-
8-9	0,99	0,72	0,88	1,00	0,59	-	-
9-10	-	0,60	0,77	1,00	-	-	-

The results in Table 3 reflects the same clear trend as identified for the total spectral energy, namely that the "large" scale spectral energy increases significantly with increasing buoyancy related turbulence production and vice versa.

Table 4. Bin specific "small" scale variance normalized with respect to "small" scale variance associated with neutral conditions.

Wind speed interval [m/s]	Very unstable	Unstable	Near neutral-unstable	Neutral	Near neutral-stable	Stable	Very stable
4-5	0,78	0,65	0,69	1,00	1,21	0,78	0,51
5-6	1,12	1,26	0,86	1,00	0,96	0,83	0,63
6-7	0,94	0,94	0,83	1,00	0,94	0,90	0,87
7-8	1,04	1,04	0,97	1,00	0,98	1,27	-
8-9	0,92	0,85	0,89	1,00	0,90	-	-
9-10	-	1,11	0,85	1,00	-	-	-

Contrary to the results presented in Tables 2 and 3, the results in Table 4 show no clear trend with regard to stability dependence of the "small" scale turbulence energy level. Therefore, with the "small" scale turbulence energy level being roughly invariant with respect stability conditions, and the "large" scale turbulence energy level being highly dependent on ABL stability conditions, the present investigation shows that the DWM split in scales roughly "matches" the split in scales between the turbulence energy-containing range and the turbulence inertial subrange, thus in turn confirming the DWM stability conjecture.

3.3. Full-scale LiDAR measurements

The full-scale LiDAR measurements analyzed in this subsection relate to the same measuring campaign as described above. As a supplement to the sonic recordings, the Nordtank turbine was equipped with a pulsed LiDAR system mounted on a platform at the rear of the turbine nacelle, thus facilitating cross sectional scanning (i.e. cross sections perpendicular to the rotor axis) of the wake affected flow field behind the turbine. A detailed description of the experimental setup can be found in [6], where also the principle of extracting the mean wind speed characteristics from LiDAR measurements recorded outside the wake regime is described. In the present analysis, mean wind speeds associated with the LiDAR recordings are derived using this technique.

The wake characteristics in downstream cross sections are resolved as based on a Cartesian scan pattern consisting of 49 measurement points (i.e. 7×7). For various stability conditions, the basic idea is to resolve and compare the *wake deficit* characteristics in the meandering frame of reference (MFoR) as well as the *wake deficit dynamics*. This is performed for otherwise similar inflow conditions; i.e. mean wind speed and mean wind direction.

The wake deficit dynamics is obtained from "instantaneous" LiDAR cross sectional scans using the wake deficit tracking procedure introduced in [18]. With the wake deficit dynamics determined, it is straight forward to perform a transformation from the fixed frame of reference (FFoR), in which the measured wake affected flow is resolved, to the MFoR.

To obtain robust results, time series with a span ranging between 3 and 5 hours is used in this part of the investigation. To ensure a sufficient amount of data complying with the requirements, this means in turn that it is necessary to merge the former two unstable classes (i.e. "very unstable" and "unstable") into a new stability class denoted "unstable collapsed". Eventually three test cases, associated with low wind conditions and therefore pronounced deficits (i.e. high trust), are selected for this part of the analysis. The characteristics of the selected time series appear from Table 5 below. As expected the ambient turbulence level is increased with ABL stability conditions changing from stable over neutral to unstable.

Table 5. Overall characteristics of test cases.

Stability condition	Mean wind speed at hub height (U_0) [m/s]	Turbulence intensity at hub height [m/s]	Length of time series [hour]
Unstable collapsed	6.82	0.15	3.3
Neutral	7.03	0.14	3.2
Very stable	6.76	0.10	5.5

The results for the wake deficits, as expressed in the MFoR, are shown in Figure 2 for downstream distances ranging between 1D and 5D, where D denotes the rotor diameter. It is evident that the deficits expressed in the MFoR are almost invariant to the ABL stability conditions, thus in this respect confirming the conjecture on which the DWM modeling of non-neutral flow fields is based.

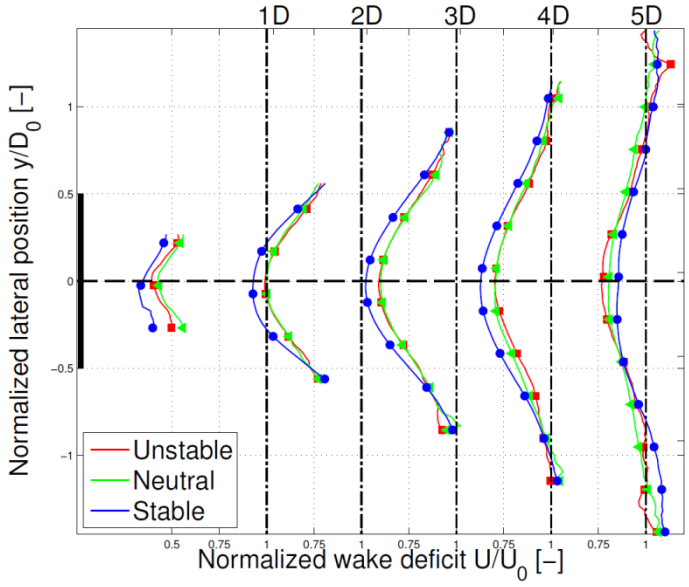

Figure 2. Normalized wake deficits in the MFoR depicted for three different stability conditions.

Turning to wake deficit dynamics, Table 6 shows the variance of the lateral wake center position for the investigated stability conditions. The lateral wake displacements are, in the context of DWM modelling , driven by the large scale lateral turbulent scales, and to facilitate direct comparisons with the inflow results given in Table 3, the results are normalized with respect to displacement variance associated with neutral conditions.

Table 6. Variance of the lateral wake center position normalized with respect to variance of the lateral wake center position associated with neutral conditions.

Downstream distance	Very unstable	Unstable	Near neutral-unstable	Neutral	Near neutral-stable	Stable	Very stable
3D	1,11	1,22	1,26	1,00	0,70	0,81	0,75
4D	1,09	1,36	1,10	1,00	0,59	0,57	0,49
5D	1,04	1,40	1,02	1,00	0,61	0,54	0,40

Qualitatively, also these results confirm the DWM conjecture stating that the wake meandering dynamics is driven by large scale turbulence structures, which in turn is highly dependent on ABL stability conditions. Although differences exists among values associated with *specific* stability

classes, a quantitative comparison of the results in Table 2 (i.e. wind bin 6-7m/s) and Table 6 shows in addition that there is a reasonable agreement between the range of "large" scale variance stability dependence and the range of wake center lateral dynamics variance stability dependence, respectively, especially considering the fact that these results originate from not identical 10-minute recordings.

4. Performance of spectral tensor including buoyancy

Having rendered probable the validity of the DWM stability conjecture, we finally explore the performance of the generalized spectral tensor described in Section 2 for various ABL stability conditions, with the potential perspective of using this spectral tensor for the required DWM large scale turbulence modelling. Figure 3 shows a fit of the spectral tensor to the measured data presented in Figure 1. Full lines represent spectral fits, and dotted lines represent measured spectra.

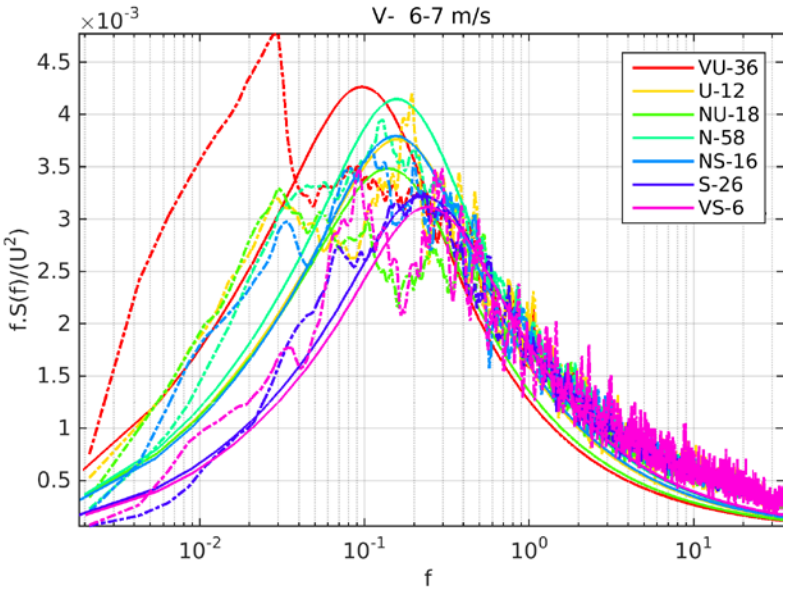

Figure 3. Spectral tensor fit to measured full-scale spectra of the lateral velocity component for various stability conditions and associated with mean wind speeds in the interval [6; 7]m/s.

Although the generalized spectral tensor is not meant to describe meso-scale effects (i.e. to include a *specific* modelling of such scales), the tensor is able to approximately capture the spectral "stability cascade" with increasing spectral length scales for increasing degree of ABL instability, and thereby paving the way for future detailed validation studies of the DWM model under non-neutral ABL stability conditions with focus on both wind turbine production and loading.

5. Conclusion

There is experimental evidence for a significant impact from atmospheric stability on wake affected flow fields in wind farms, which in turn affects both wind farm production and loading of the individual turbines. By analyzing an extensive amount of full-scale data based on both sonic measurements and LiDAR measurements, we have demonstrated the validity a conjecture stating that, in the context of DWM modelling, ABL stability impacts *only* the "large" turbulence scales constituting the meandering regime, whereas the "small" scale turbulence regime responsible for wake deficit expansion and attenuation in the MFoR can be considered invariant with respect to ABL stability conditions. Generalisation of the DWM model to non-neutral conditions is thus straight forward, and facilitated by the recent development of a spectral tensor including buoyancy effects.

Acknowledgments
The EUDP project "Impact of atmospheric stability conditions on wind farm loading and production" under contract 64010-0462 is acknowledged for financial support and thus for making this study possible.

References
[1] Hansen, K.S.; Barthelmie, R.; Ott, S. and Larsen, G.C. (2012). Park power deficit due to atmospheric stability. The Science of Making Torque from Wind, October 9-11, Oldenburg, Germany.
[2] Hansen, K.S.; Larsen, G.C. and Ott, S. (2014). Dependence of offshore wind turbine fatigue loads on atmospheric stratification. The Science of Making Torque from Wind 2012, June 17-20, Lyngby, Denmark.
[3] Larsen, G.C.; Larsen, T.J.; Mann, J.; Peña, A.; Hansen, K.S. and Madsen, H.Aa. (2009) The dependence of wake losses on atmospheric stability characteristics. EUROMECH Colloquium 508 on Wind Turbine Wakes, pp. 35–37.
[4] Keck, R.-E.; de Maré, M.; Churchfield, M.J.; Lee, S.; Larsen, G.C. and Madsen H.Aa. (2014). On atmospheric stability in the dynamic wake meandering model. Wind Energy, Volume 17, Issue 11, pages 1689–1710.
[5] Chougule, A. (2013). Influence of atmospheric stability on the spatial structure of turbulence. DTU Ph.D. thesis, 109p.
[6] Machefaux, E.; Larsen, G.C.; Koblitz, T.; Troldborg, N.; Kelly, M.; Chougule, A.; Hansen, K.S. and Rodrigo, J.S. (2014). Experimental and numerical study of the atmospheric stability impact on wind turbine wake. Accepted for publication in Wind Energy.
[7] Larsen, G.C.; Madsen, H.Aa.; Thomsen, K. and Larsen, T.J. (2008). Wake Meandering: A Pragmatic Approach. Wind Energy, Volume 11, Issue 4, pages 377–395.
[8] Madsen, H.Aa.; Larsen, G.C.; Larsen, T.J.; Troldborg, N. and Mikkelsen R. (2010). Calibration and Validation of the Dynamic Wake Meandering Model for Implementation in an Aeroelastic Code. Journal of Solar Energy Engineering, Vol. 132(4), 041014.
[9] Bingöl, F.; Mann, J. and Larsen G.C. (2010). LiDAR Measurements of Wake Dynamics, Part 1: One Dimensional Scanning. Wind Energy, Volume 13, Issue 1, pages 51–61.
[10] Larsen, T.J.; Madsen, H.Aa.; Larsen, G.C. and Hansen, K.S. (2013). Validation of the Dynamic Wake Meander Model for Loads and Power Production in the Egmond aan Zee Wind Farm. Wind Energy, Volume 16, Issue 4, pages 605–624.
[11] Larsen, G.C.; Larsen T.J.; Mann, J.; Peña, A.; Hansen, K.S. and Madsen, H.Aa. (2009). The dependence of wake losses on atmospheric stability characteristics. EUROMECH Colloquium 508 on Wind Turbine Wakes; 35–37.
[12] Mann, J. (1994). The Spatial Structure of Neutral Atmospheric Surface-Layer Turbulence. J. of Fluid Mech., 273, 141-168.
[13] von Kármán, T. (1948). Progress in the statistical theory of turbulence. Proc. Nat. Acad. Sci., 34:530–539.
[14] Kaimal, J.C. and Finnigan, J.J. (1994). Atmospheric Boundary layer Flows – Their structure and Measurement. Oxford University Press.
[15] Kaimal, J.C.; Wyngaard, J.C.; Izumi, Y. and Coté, O.R. (1972). Spectral characteristics of surface-layer turbulence. Q. J. R. Meteorol. Soc., 98(417):563–589. doi:10.1002/qj.49709841707.
[16] Mann, J. (1998). Wind field simulation, Prob. Eng. Mech. 13(4), pp. 269–282.
[17] Peña, A.; Gryning, S.E. and Mann J. (2010). On the length-scale of the wind profile. Quarterly Journal of the Royal Meteorological Society; 136(653); 2119–2131.
[18] Trujillo, J.; Bingöl, F.; Larsen, G.C. and Mann, J. (2011). Light detection and ranging measurements of wake dynamics. Part II: two-dimensional scanning. Wind Energy, Volume 14, Issue 1, pages 61–75.